https://doi.org/10.5194/angeo-2019-160
Preprint. Discussion started: 18 December 2019

Annales Geophysicae Discussions
Open Access
EGU

Modeling Total Electron Content derived from radio occultation measurements by COSMIC satellites over the African Region

Patrick Mungufeni[1], Claudia Stolle[2,3], Sripathi Samireddipalle[4],Yenca Migoya-Orué[5], and Yong Ha Kim[1]

[1]Department of Astronomy and Space Science, Chungnam National University, Daejeon, South Korea
[2]GFZ German Research Centre for Geosciences, Potsdam, Germany
[3]Faculty of Sciences, University of Potsdam, Potsdam, Germany
[4]Indian Institute of Geomagnetism, New Panvel, India
[5]T/ICT4D laboratory of the Abdus Salam International Center for Theoretical Physics, 34151 Trieste, Italy

Abstract

This study developed a model of Total Electron Content (TEC) over the African region. The TEC data were derived from radio occultation measurements done by the Constellation Observing System for Meteorology, Ionosphere, and Climate (COSMIC) satellites. Geomagnetically quiet time (Kp < 3 and *Dst* > -20 nT) data during the years 2008 - 2011, and 2013 – 2017 were binned according to local time, seasons, solar flux level, geographic longitude, and dip latitude. Cubic B splines were fitted to the binned data to obtain the model. The model was validated using TEC data of the years 2012 and 2018. The validation exercise revealed that, approximation of observed TEC data by our model produces root mean squared error of 4.8 TECU. Moreover, the modeled TEC data correlated highly with the observed TEC data (r = 0.93). Our model is the first attempt to predict TECs over the entire African region by using extensive COSMIC TEC measurements. Due to the extensive input data and the good modeling technique, we

https://doi.org/10.5194/angeo-2019-160
Preprint. Discussion started: 18 December 2019

Annales Geophysicae Discussions

were able to reproduce the well-known features such as local time, seasonal, solar activity, and spatial variations of TEC over the African region.

1. Introduction

Among the error sources that affect positioning using Global Navigation Satellite Systems (GNSS) are the propagation medium related errors. In particular, the ionospheric refraction is the largest contributor of the user equivalent range error. This type of frequency dependent error can virtually be eliminated in dual frequency receivers by differential techniques (Hofmann-Wellenhof et al., 2007). For the case of single frequency receivers, the GNSS broadcast message includes the parameters of an ionospheric model which can be used to compute and correct the ionospheric effects (Guochang, 2007). For instance, the Global Positioning System (GPS) uses the Klobuchar model which represents the zenith delay as a constant value at night and a half cosine function during day (Leva et al., 2006). In the framework of the European Galileo constellation, the NeQuick G based on NeQuick2 model has been proposed to be used for single frequency positioning (Nava et al., 2008). The NeQuick is a three-dimensional, time dependent ionospheric electron density model developed by the Aeronomy and Radio Propagation Laboratory (ARPL) of the Abdus Salam International Center for Theoretical Physics (ICTP) in Trieste, Italy and the Institute for Geophysics, Astrophysics and Meteorology of the University of Graz, Austria (Nava et al., 2008). In addition to using models to reduce ionospheric refraction errors, Space Based Augumentation Systems (SBAS) such as the Wide Area Augmentation System (WAAS), the EuropeanGeostationary Navigation Overlay Service (EGNOS), and the GPS And Geo-Augmented Navigation (GAGAN) are also used (Hofmann-Wellenhof et al., 2007).

For the international standard specification of ionospheric parameters (such as electron and ion densities, temperatures, velocities), the Committee on Space Research (COSPAR) and the International Union of Radio Science (URSI) recommended the International Reference Ionosphere Model (IRI) (Bilitza, 2001). The model is primarily based on all available experimental data (ground and space based) sources. However,

https://doi.org/10.5194/angeo-2019-160
Preprint. Discussion started: 18 December 2019

theoretical considerations have been used in bridging data gaps and for internal consistency checks (Bilitza, 2001).

The ionospheric Total Electron Content (TEC) is one of the important descriptive physical quantities of the ionosphere (Rama Rao et al., 1997; Ercha et al., 2012). The GNSS measurements obtained from the global and regional networks of International GNSS Service (IGS) ground receivers have become a major source of TEC data. As one of the IGS analysiscenters, Center for Orbit Determination in Europe (CODE) provides Global Ionospheric TEC data Map (GIM) daily usingthe GNSS data collected from over 200 tracking stations of IGS and other institutions. Several studies have used Global Ionospheric TEC data Maps (GIMs) from CODE and other IGS analysis centers such as the Jet Propulsion Laboratory (JPL) to construct TEC models (Jakowski et al. 2011a; Mukhtarov et al. 2013; Ercha et al. 2012; Sun et al., 2017). Jakowski et al. (2011a) proposed the Global Neustrelitz TEC Model (NTCM-GL) that describes theaverage TEC under quiet geomagnetic conditions. The NTCM-GL was developed using GIMs during 1998 - 2007 provided byCODE. A global background TEC model was also built using CODE GIMs by Mukhtarov et al. (2013). The model describes the climatological behavior of the ionosphere. The GIMs from JPL were used by Ercha et al. (2012) to construct a GIM using Empirical Orthogonal Function (EOF) analysis method. The Taiwan Ionosphere Group for Education and Research constructeda GIM model from GNSS and the Constellation Observing System for Meteorology, Ionosphere, and Climate (COSMIC) GPSradio occultation observations (Sun et al., 2017). The map of all the averaged Root Mean Squared (RMS) error values of CODE GIMs during the years 2010 - 2012 presented by Najman and Kos (2014) showed high values over low latitude African regions. This could be due to the poor distribution of IGS tracking stations over Africa and anomalies in the ionosphere relatedto the geographic and geomagnetic location.

In addition to the existing GIMs discussed in the previous paragraph, regional TEC maps and models have also been constructed. In comparison with the GIM model, regional TEC models might have better accuracy over the particular region for which it was constructed. Opperman (2008) stated that the higher time and spatial resolution

https://doi.org/10.5194/angeo-2019-160
Preprint. Discussion started: 18 December 2019

imaging achievable with regional models permits the analysis of localized ionospheric structure and dynamics not observable on a global scale model. Examples of studies that developed TEC models over some parts of Africa are the following. A neural network modelof GNSS - vertical TEC (GNSS-VTEC) over Nigeria was developed by Okoh et al. (2016) using all available GNSS data fromthe Nigerian GNSS Permanent Network (NIGNET). An adjusted spherical harmonic-based TEC model was developed by Opperman (2008) using a network of South African dual frequency GPS receivers. Habarulema (2011) presented the Southern Africa TEC prediction (SATECP) model that was based on the Neural Network technique. The SATECP generates TEC predictions as function of input parameters, namely, local time, day number of the year, solar and magnetic activity levels, and the geographical location. A neural network based ionospheric model was developed using GPS-TEC data over the East African sector by Tebabal et al. (2019).

Due to the lack of a dense network of ground-based GNSS receivers, it has not been possible to construct a regional TEC model over the entire African region. Considering that the regional models discussed in the previous paragraph utilized ground-based measurements, it is important to take advantage of space-based measurements to develop TEC model over the entire African region. Therefore, in this study, we proposed a regional TEC model for the African region using COSMIC data. In section 2, the data and methods of analysis that were used in the study are described. The model used in the study is described in section 3. We present comparison between the observed and modeled TEC in section 4. The model validation and the conclusions of the study are presented in sections 5 and 6, respectively.

2. The Data and methods

2.1 Data sources

In order to overcome the problem of lack of a dense network of ground based GNSS receivers over the African region, this study used TEC data obtained from radio occultation measurements done by the COSMIC satellites. The integrated electron density (integration being done up to the altitudes of the COSMIC satellites) which is being referred to as TEC in this study can be obtained from ionPrf files which are

https://doi.org/10.5194/angeo-2019-160
Preprint. Discussion started: 18 December 2019

processed at the COSMIC Data Analysis and Archive Centre (CDAAC)(http://cosmic-io.cosmic.ucar.edu/cdaac/index.html). The TEC for the individual occultation events were assigned to the geographic coordinates of NmF2 in the same file. Analysis of coincident ground-based GNSS TEC and TEC from COSMIC occultation data by Mungufeni et al. (2019) reveals that the upper quartile of the differences between the two data sets may reach up to ~11 TECU over the northern crest of the Equatorial Ionization Anomaly. Over the southern mid-latitude region, the differences were low (~4 TECU). Since the magnitudes of the TEC obtained from COSMIC occultation measurements are close to ground based GNSS TEC, we used the former to develop a TEC model over the African region.

During geomagnetic storms, the variations in zonal electric fields and composition of the neutral atmosphere contribute significantly to the occurrence of negative and positive ionospheric storm effects in the low latitude region (Rishbeth and Garriot, 1969; Buonsanto, 1999; Adewale et al., 2011). Therefore, since the ionosphere changes in a complex manner during geomagnetic storms, we only considered data on quiet days. The quiet geomagnetic days were identified by examining the 3 hourly Kp and Disturbance storm time (Dst) indices that were obtained from the World Data Center of Kyoto, Japan (http://swdcwww.kugi.kyoto-u.ac.jp/). A day was considered to be quiet if all the 8 Kp values in that day were ≤ 3. In addition to satisfying this condition, all the hourly values of Dst in that day should also have values ≥ -20 nT. The two conditions were applied to ensure that both low and mid/sub-auroral latitude geomagnetic disturbances are detected by Dst and Kp indices, respectively. In future, we intend to use TEC data during disturbed geomagnetic conditions to construct a TEC model duringgeomagnetically disturbed conditions.

2.2 Methods of Data Analysis

The TEC data during the years 2008 - 2011 and 2013 - 2017 were used for developing the TEC model over the African region. Due to the adequate data needed to develop an empirical model, we only reserved the data of the years 2012 and 2018 for validation. The period considered in this study represents data of both low and high

https://doi.org/10.5194/angeo-2019-160
Preprint. Discussion started: 18 December 2019

solar activity in sunspot cycles 23 and 24. The data within geographic latitude and longitude ranges of -35 – 35° and -15 – 60°, respectively, were used to cover the African region. Since many structural and dynamical features of the ionized and neutral upper atmosphere are strongly organized by the geomagnetic field (e.g. Emmert et al., 2010), we computed the dip latitudes, ϕ of the TEC data points using

$$\phi = \tan^{-1}\left(\frac{\tan(I)}{2}\right), \tag{1}$$

where *I* is the geomagnetic field inclination angle. The values of *I* were computed using the International Geomagnetic Reference Field model of 2012 (Thébault et al., 2015). The dip latitude values were in the range of -48 - 34.8°.

The TEC data were binned in grids with resolution of 15° in geographic longitude and the dip latitude resolution was varied as shown later in this paragraph since the dip latitude contours far from the dip equator are widely separated. In order to observe small scale ionospheric structures smaller grid resolutions would be ideal. The problem that might arise when a smaller grid resolution is applied is data gaps in some grids. The choice of the grid resolution in this study aimed at minimizing data gaps at grids. Within the time difference of the 15° longitude bin, the TEC might not vary greatly. On the other hand, the latitudinal grid resolution was reduced 15° to 5°for dip latitude range of -20 – 20° to reflect rapid variations of TEC latitudinally, and the latitudinal resolution was increased to 6° for dip latitude in the range of -20 - -32° and 20 – 26°. It was further increased to 8° for dip latitude values < -32° as well as dip latitude values > 26°.

Table 1 presents the number of days per year when there were TEC data over the African region. Since there are many geomagnetically disturbed days in high solar activity years (2011 - 2016), the number of days with data is also reduced in such years compared to low solar activity years (2008 - 2010, 2018). The total number of TEC data values available at all the grids were 140,026. These data values were further binned as follows.

https://doi.org/10.5194/angeo-2019-160
Preprint. Discussion started: 18 December 2019

Annales Geophysicae Discussions

For each spatial grid cell, the data were binned at 1 hour interval. TEC values within the bins were averaged to yield 1 hour resolution TEC data over the grids. TEC data for the different days were binned according to F10.7 flux of that day. The F10.7 flux indices were obtained from the Space Weather Prediction Center (SWPC) of the National Oceanic and Space Administration (NOAA) (http://www.swpc.noaa.gov/). The F10.7 flux ranges for low solar activity (LSA), medium solar activity (MSA), and high solar activity (HSA) were < 76, 76 - 108, and >108 sfu, respectively. The boundary values 76 and 108 sfu of theF10.7 flux ranges correspond to the 75*th* and 25*th* percentiles of all F10.7 flux values on the days in low (2008 - 2010, 2017 -2018) and high (2012 - 2015) solar activity years, respectively.

The data within a specific solar flux bin were further binned based on months of a year. The average of the corresponding F10.7 flux of the days used to represent seasonal TEC were determined and used to capture the variation of TEC with solar flux. Table 2 presents the average F10.7 flux values that were determined in the months of a year. In summary, after binning the 140,026 TEC data values into 5 longitudinal, 14 latitudinal, 36 solar flux, 12 monthly, and 24 hourly bins, a total of 60,480 TEC data values were obtained and used to determine the model coefficients.

Table 1: Distribution of number of days with data

Year	Number of days with data
2008	219
2009	293
2010	235
2011	174
2012	169
2013	185
2014	164
2015	128
2016	151
2017	154
2018	211

https://doi.org/10.5194/angeo-2019-160
Preprint. Discussion started: 18 December 2019

Annales Geophysicae Discussions Open Access EGU

Table 2: Average monthly F10.7 flux values used in the study

Month	F10.7 flux value		
	LSA	MSA	HSA
January	71.1	85.2	144.8
February	71.1	88.8	132.7
March	69.7	86.3	132.8
April	70.9	92.1	132.4
May	70.1	93.9	131.5
June	69.1	93.1	124.6
July	67.9	90.2	134.6
August	67.4	92.2	119.1
September	69.2	88.0	125.8
October	69.8	82.7	131.7
November	71.6	83.1	144.0
December	70.6	83.1	143.1

3. The Model

The TEC over the African region was expressed as

$$TEC(t,d,F,\lambda,\phi) = \sum_{i=1}^{24}\sum_{j=1}^{12}\sum_{k=1}^{3}\sum_{l=1}^{5}\sum_{m=1}^{14} a_{ijklm} \times N_i(t) \times N_j(d) \times N_k(F) \times N_l(\lambda) \times N_m(\phi) \quad (2)$$

where the linear model coefficients a_{ijklm} were determined by the least square fitting procedure to the 60,480 TEC data values as in Abdu et al. (2003); Jakowski et al. (2011b); Mungufeni et al. (2015). In Equation 2, $N_i(t)$, $N_j(d)$, $N_k(F)$, $N_l(\lambda)$, and $N_m(\phi)$ are cubic B splines to represent variations of TEC with local time, seasons, solar flux level, longitude, and dip latitude respectively. Most of the cubic B splines were of order 2, except those used to represent LT and latitudinal variations which were of order 4. The order of splines used to represent LT and latitude was higher to cater for the rapid variations of TEC with these two parameters. Twenty four local time nodes 1, 2, ..., 24 were used. For simple interpolation between months, seasonal/monthly nodes were placed at the 15th day of each month. Solar flux nodes used in the various months are as shown in Table 2. The longitudinal nodes were separated by 15^{o} and placed at longitudes -7.5, 7.5, ..., 52.5 degrees, while the latitudinal nodes were placed at dip latitudes -44, -36, -29, -23, -17.5, -12.5, -7.5, -2.5, 2.5, 7.5, 12.5, 17.5, 23, and 30 degrees.

4. Comparison of Observed and Modeled TEC

In order to appreciate the fact that cubic B splines are very good fits to observed data, we compared the observed binned data that were used in solving equation 1 and the corresponding modeled TEC data. It is important to note that validation using data that was not included during modeling is provided in section 5. Panels in column (i) of Figure 1 present the observed binned TEC data while column (ii) presents the corresponding modeled TEC data. In column (iii), we present Global Ionosphere Map (GIM) TEC (GIM-TEC) produced by Center for Orbit Determination in Europe (CODE). The daily GIM-TEC values are derived using the GNSS data collected from over 200 tracking stations of IGS and other institutions. In Figure 1, rows (a), (b), and (c) correspond to LSA, MSA, and HSA, respectively. It should be noted that the GIM-TEC presented on panels in rows (b) and (c) were for those on dates of March 21, 2018 and March 21, 2012, respectively. The horizontal magenta lines in Figure 1 and later also in Figure 2 indicate the location of 0^{o} dip latitude on the corresponding panel.

As expected, Figure 1 clearly shows that the corresponding modeled TEC almost perfectly matches the observed binned TEC. The variations of the ionosphere with local time, solar flux level as well as location that are exhibited in Figure 1 gives the confidence of relying on the binned data as a good representation of the ionosphere. The physical explanations for these variations are as follows. The increase of both observed and modeled TEC that occurs when solar flux level increases is usually

https://doi.org/10.5194/angeo-2019-160
Preprint. Discussion started: 18 December 2019

Annales Geophysicae Discussions
Open Access
EGU

attributed to increased ionizing radiations in X-ray and Extreme Ultra-Violet (EUV) bands, which inturn leads to increased TEC in the ionosphere (Hargreaves, 1992).

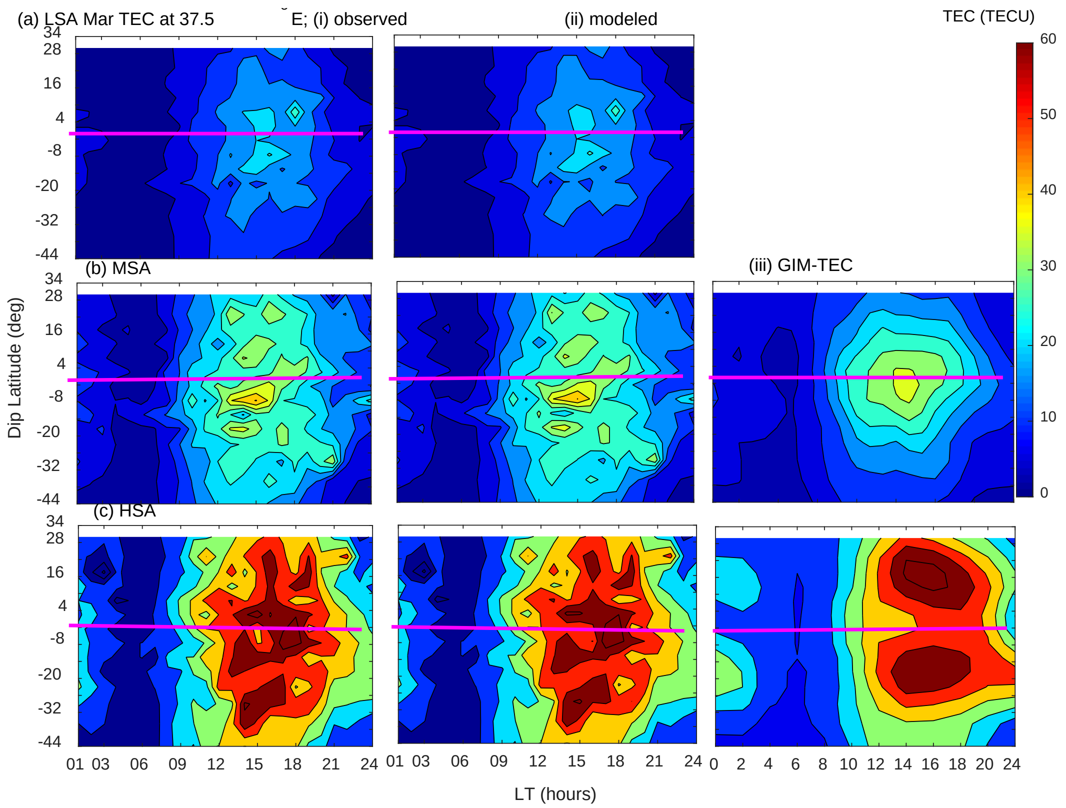

Figure 1. Variation of TEC as a function of dip latitude and local time in March equinox at 37.5^o E. Panels in rows (a) - (c) correspond to LSA, MSA, and HSA, respectively, while panels in columns (i) - (iii) correspond to observed binned, modeled TEC, and GIM-TEC, respectively. Magenta line indicates 0^o dip latitude.

The diurnal variation of TEC matches very well with the variation of photo-ionising radiations. At sunrise, the electron density begins to increase rapidly owing to photo-ionization (Schunk and Nagy, 2009). After this initial increase at sunrise, electron density displays a slow rise throughout the day, and then it decays at sunset as the photo-ionization source disappears. Another diurnal feature of variation of TEC exhibited in Figure 1 is the existence of a secondary maximum of TEC. This can clearly be seen in panels of row (c) at latitudes of -20 and 4 degrees. Along these latitudes at

https://doi.org/10.5194/angeo-2019-160
Preprint. Discussion started: 18 December 2019

18:00 LT there is a decrease in TEC followed by an increase. Due to poor distribution of IGS receivers over the region of study, the GIM-TEC did not exhibit the secondary TEC maximum seen in observed and modeled TEC data.

The formation of a secondary maximum of TEC that was mentioned previously may be explained as follows. During the day, the thermospheric wind generates a dynamo electric field in the lower ionosphere that is eastward (Schunk and Nagy, 2009). The eastward electricfield, E in combination with the northward geomagnetic field, B produces an upward E×B drift of the F region plasma. As the ionosphere co-rotates with the Earth toward dusk, the zonal (eastward) component of the neutral wind increases. The increased eastward wind component, in combination with the sharp day-night conductivity gradient across the terminator leads to the pre-reversal enhancement in the eastward electric field (Batista et al., 1986; Schunk and Nagy, 2009). The F layer therefore rises as the ionosphere co-rotates into darkness. Although in the absence of sunlight after sunset, the lower ionosphere rapidly decays, there exists high electron density at high altitudes, yielding the secondary maximum in TEC.

Panels in rows (b) and (c) of Figure 1 demonstrate the existence of the EIA region, where there exist two belts of high electron density on both sides of 0º dip latitude. It should be noted that at MSA, this feature is not seen in the GIM-TEC data. The EIA is usually attributed to the upward $E \times B$ drift which lifts plasma to higher altitudes. The plasma then diffuses north and south along magnetic field lines. Due to gravity and pressure gradient forces, there is also a downward diffusion of plasma. The net effect is the formation of the EIA region (Appleton, 1946). The panels in rows (b) and (c) of Figure 1 (columns (i) and (ii)) indicate that there are several crests on both sides of 0º dip latitude. On the other hand, GIM-TEC did not exhibit this feature. Observations of several crests on both sides of the dip equator were reported over our study region by the previous studies done by Bolaji et al. (2017) and Mungufeni et al. (2018). The authors attributed creation of several crests on either side of the magnetic equator due to inconsistent transfer of plasma during diffusion along geomagnetic magnetic field lines. Another feature of EIA that can be seen on panels in rows (b) and (c) of Figure 1 is the asymmetry of the crests. The asymmetry of EIA crests is not exhibited in GIM-

https://doi.org/10.5194/angeo-2019-160
Preprint. Discussion started: 18 December 2019

TEC. Along 120° longitude sector Zhang et al. (2009) reported the asymmetry of EIA crests. As described later at the end of this section, the direction of neutral meridional winds in March may favour high values of electron density over the southern crest.

Generally, Figure 1 shows that, the locations outside the EIA region have lower TEC values compared to locations around and within the EIA region. The low values of TEC over locations outside the EIA region might be due to lower elevation angle of solar radiation flux which is responsible for creation of electrons (Schunk and Nagy, 2009). The solar radiation flux is usually low for locations far from the sub-solar point. The latter situation is dominant over locations outside the EIA region, especially in March. The closeness of the sub-solar point to the locations within the EIA regions result into high solar radiations over these locations. As a result, high TEC values were observed over locations within the EIA region. Overall, unlike the observed binned and our modeled TEC, the GIM-TEC did not exhibit most of the well known ionospheric features such as occurrence of secondary TEC peak and asymmetry of EIA over the region. Therefore, this necessitates our modeling effort.

To demonstrate that the modeled TEC captures TEC variation with seasons, we present Figure 2. In the figure, columns (i) and (ii) present observed binned and the corresponding modeled TEC respectively. Moreover, rows (a) - (d) present TEC data during March, June, September and December, respectively.

https://doi.org/10.5194/angeo-2019-160
Preprint. Discussion started: 18 December 2019

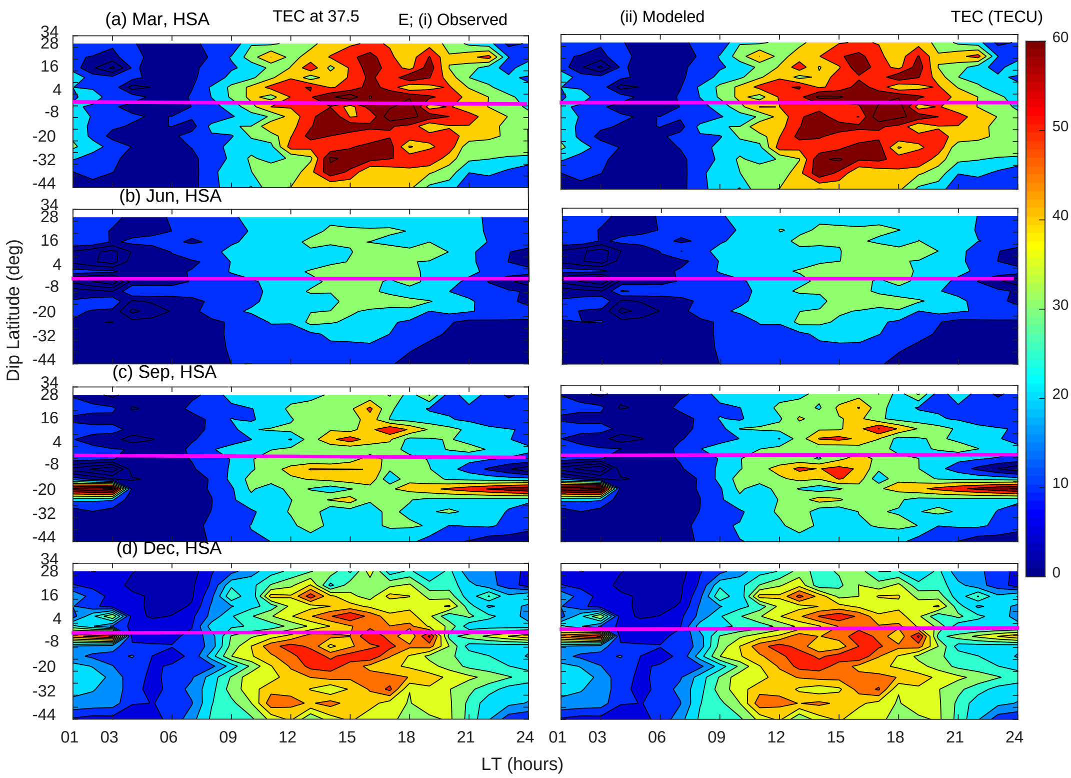

Figure 2. Variation of TEC as a function of latitude and local time in HSA at 37.5^{o}E. Panels in rows (a) - (d) are for March equinox, Junesolstice, September equinox, and December solstice respectively, while panels in columns (i) and (ii) are observed binned and modeled TEC respectively. Magenta line indicates 0^o dip latitude.

As already observed in Figure 1, it can clearly be seen from Figure2 that the modeled TEC almost perfectly matches the observed TEC data. Among the many features of TEC exhibited by both observed and modeled TEC data, we would like to emphasize the (i) equinoxial asymmetry of TEC, (ii) occurrence of lowest TEC in June solstice, and (iii) high values of TEC in December. Features (ii) and (iii) were recently reported based on a similar data by Mungufeni et al. (2019). The reader may refer to this study for more discussions. Mungufeni et al. (2016a) observed equinoxial asymmetry when studying ionospheric irregularities over the African low latitude region. They observed over the East African region that, the irregularity strength in March equinox was higher than that

https://doi.org/10.5194/angeo-2019-160
Preprint. Discussion started: 18 December 2019

in September equinox. They attributed the equinoxial asymmetry to meridional winds in March which might blow northward. Such a direction would lift plasma up where recombination is not common. On the other hand, in September, the winds might blow southward. This could lead to recombination at low altitudes.

5. Model Validation

In addition to comparing observed binned TEC with the corresponding modeled TEC, we validated our model using observed TEC in the years 2012 and 2018. The data during these two years were not used in developing the model. The TEC data in the years 2012 and 2018 were binned according to local time and spatially in a similar manner to that mentioned in subsection 2.2. The corresponding local time, day of the year, solar flux, and spatial coordinates of the data were noted and then used to generate the corresponding modeled TEC. Figure 3 presents a scatter plot showing the observed TEC against the corresponding modeled TEC. The red line in the figure indicates linear least squares fit to the data in the panel. Furthermore, indicated in Figure3 are; (i) the correlation coefficients, r, (ii) the r squared values, (iii) the number of data points, n plotted and (iv) the root meansquared error, RMSE when the modeled TEC is used to represent the observed TEC.

https://doi.org/10.5194/angeo-2019-160
Preprint. Discussion started: 18 December 2019

Annales Geophysicae
Discussions
Open Access
EGU

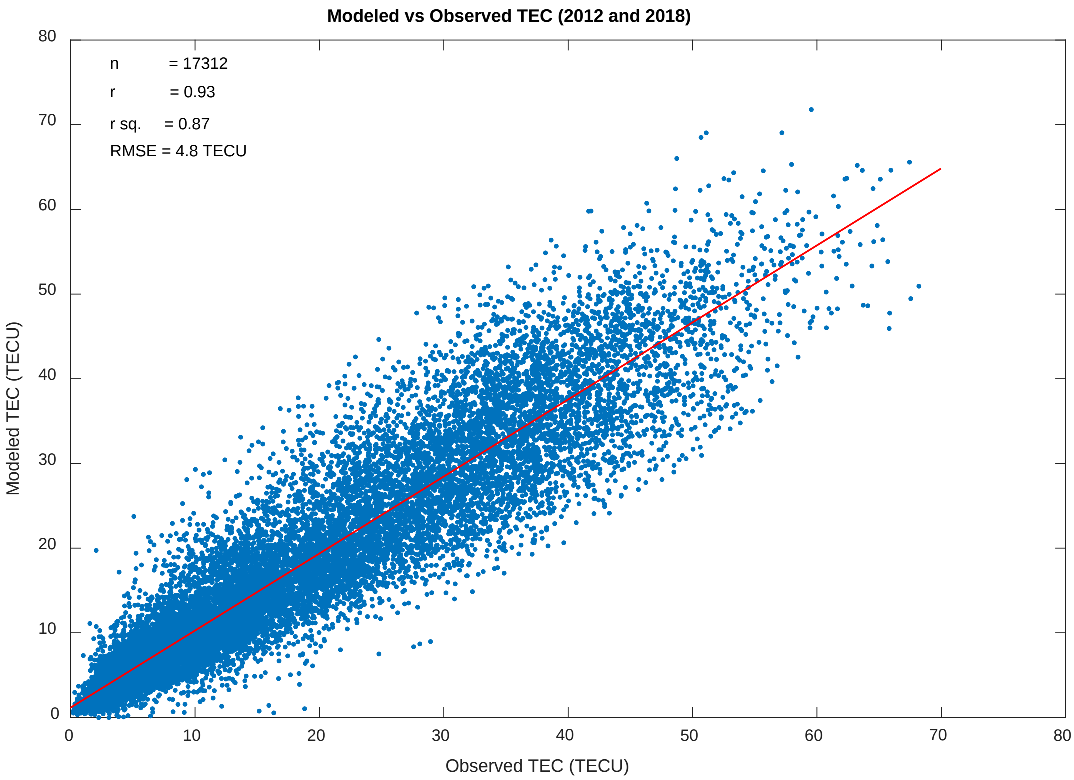

Figure 3. Scatter plot of observed TEC against modeled TEC.

The following observations can be noted from Figure 3. (i) The modeled TEC correlates highly (r ~0.93) with the observed TEC. (ii) The r squared values indicate that high proportions (~87 %) of the variations in the observed TEC can be predicted by the modeled TEC. (iii) The RMSE value of 4.8 TECU signify that the modeled TEC closely approximates the observedTEC.

In order to show that the observed and modeled TEC have similar magnitudes in addition to their similar variation depicted in Figure 3, we computed the differences between corresponding values of the data plotted in the figure. These were referred to as errors. Figure 4 presents the distribution of the number of observed errors. It can be seen from the figure, the errors are randomly distributed since the distribution curve is

https://doi.org/10.5194/angeo-2019-160
Preprint. Discussion started: 18 December 2019

Annales Geophysicae Discussions

symmetric about 0 TECU. Indeed, the magnitudes of the modeled TEC values are close to that of the observed TEC since the majority of the error values are close to zero.

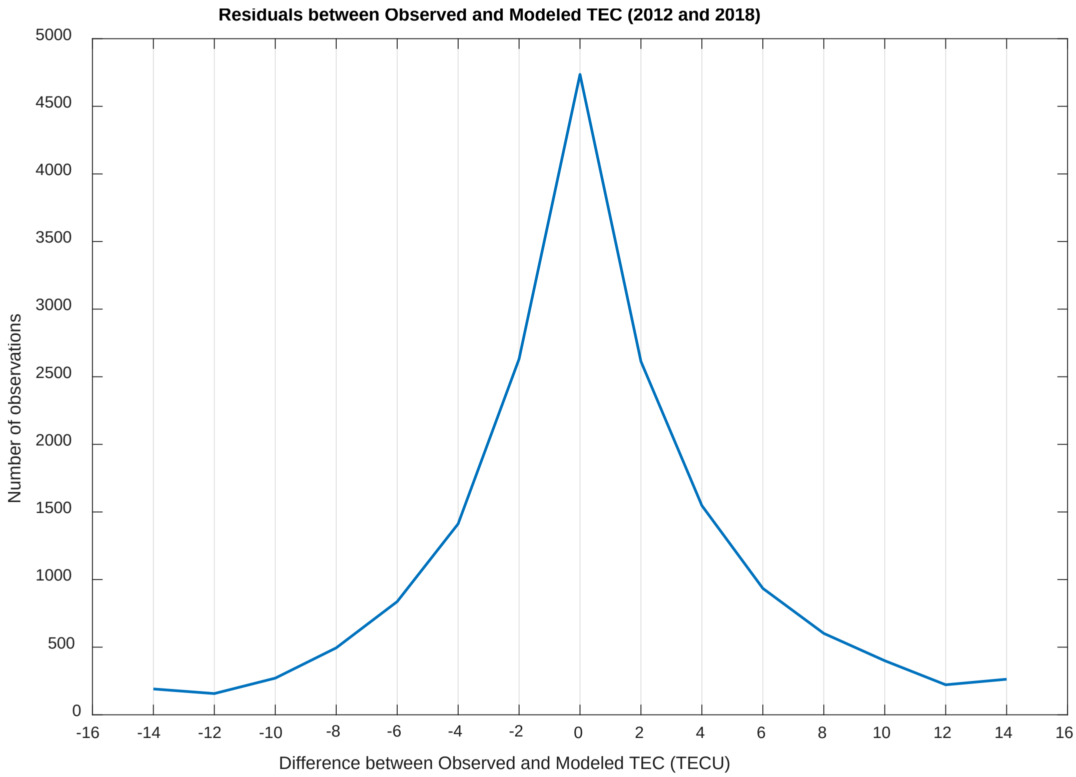

Figure 4. Distribution of the number of observed errors (difference between observed and modeled TEC).

It appears that the performance of our model in predicting the observed TEC data is better than that of the previous studies. For example, the regional Southern Africa TEC prediction (SATECP) model developed by Habarulema (2011) reveals the best correlation coefficient as 0.89, while our study obtained 0.93. Another example that shows our model performs well can be realized in comparing the RMSE of the neural network model of GNSS-VTEC over Nigeria developed by Okoh et al. (2016). Their RMSE value was 8.5 TECU, while that of our study was 4.8 TECU. These examples demonstrate the good modeling technique used in our study.

https://doi.org/10.5194/angeo-2019-160
Preprint. Discussion started: 18 December 2019

6. Conclusions

This study developed a model of TEC measured by COSMIC satellites. The TEC data were binned according to local time, seasons, solar flux level and spatially. The coefficients of cubic B splines that were fitted to the binned data were determined by means of the least square procedure. As expected, the modeled TEC almost perfectly matched the corresponding observed binned TEC data. The model was validated with independent data that were not used in model development. The validation revealed that (i) the observed and the modeled TEC correlate highly (*r* = 0:93), (ii) the coefficient of determination R^2 which is the proportion of variance in the observed data predicted by our model was 87 %, and (iii) the modeled TEC closely approximates the observed TEC (RMSE of 4.8 TECU). This is the first study to present empirical TEC model based on extensive TEC measurements over the entire African region. Due to the extensive input data and the good modeling technique, we were able to reproduce the wel- known features of TEC variation over the African region. Such a model with low RMSE could easily be adopted in future by single frequency GNSS users to correct ionospheric errors over the entire African region.

Acknowledgments

This study received financial support from research number, 018-1370-20 in the department of Astronomy and Space Science of Chungnam National University which was awarded by the Air Force Research Laboratory of the United States of America. Dst data is provided by the World Data Center for Geomagnetism at Kyoto (http://swdcwww.kugi.kyoto-u.ac.jp/). Kp data isprovided by GFZ Potsdam, ftp://ftp.gfz-potsdam.de/pub/home/obs/kp-ap/. F10.7 flux data was obtained from http://www.swpc.noaa.gov/,while ionPrf files used to derive COSMIC TEC were obtained from http://cosmic-io.cosmic.ucar.edu/cdaac/index.html.

References

Abdu, M. A., Souza, J. R., Batista, I. S., and Sobral, J. H. A.: Equatorial spread F

https://doi.org/10.5194/angeo-2019-160
Preprint. Discussion started: 18 December 2019

statistics and empirical representation for IRI: A regionalmodel for the Brazilian longitude sector, Adv. Space Res., 31, pp. 703 – 716, 2003.

Adewale, A. O., Oyeyemi, E. O., Adeloye, A. B., Ngwira, C. M., and Athieno, R.: Responses of equatorial F region to different geomagneticstorms observed by GPS in the African sector, J. Geophys. Res., 116, A12319, doi:10.1029/2011JA016998, 2011.

Appleton, E. V.: Two Anomalies in the Ionosphere, Nature, p. 691, 1946.

Batista, I. S., Abdu, M. A., and Bittencourt, J. A.: Equatorial F region vertical plasma drifts: seasonal and longitudinal asymmetries in the American sector, J. Geophys. Res., 91, pp. 12055 – 12064, 1986.

Bilitza, D.: International Reference Ionosphere 2000, Radio Sci., 36, pp. 757 – 767, 2001.

Bolaji, O., Owolabi, O., Falayi, E., Jimoh, E., Kotoye, A., Odeyemi, O., Rabiu, B., Doherty, P., Yizengaw, E., Yamazaki, Y., Adeniyi, J., t Kaka, R., and Onanuga, K.: Observations of equatorial ionization anomaly over Africa and Middle East during a year of deep minimum, Ann. Geophys., 35, pp. 123 – 132, 2017.

Buonsanto, M. J.: Ionospheric Storms – A Review, Space Sci. Rev., 88, pp. 563–601, 1999.

Emmert, J. T., Richmond, A. D., and Drob, D. P.: Statistical analysis of the correlation between the equatorial electrojet and the occurrence of the equatorial ionisation anomaly over the East African sector, J. Geophys. Res., 15; A08322; doi:10.1029/2010JA015326, 2010.

Ercha, A., Zhang, D., Ridley, A. J., Xiao, Z., and Hao, Y.: A global model: Empirical orthogonal function analysis of total electron content 1999–2009 data, J. Geophys. Res., 117, doi:10.1029/2011JA017238, 2012.

Guochang, X.: GPS. Theory, Algorithms, and Applications, Springer-Verlag, pp. 43, 2007.

https://doi.org/10.5194/angeo-2019-160
Preprint. Discussion started: 18 December 2019

Annales Geophysicae Discussions

Habarulema, J.B., M. L. O. B.: Regional GPS TEC modeling; attempted spatial and temporal extrapolation of TEC using neural networks, J. Geophys Res: Space Phys., 116, A04314, 2011.

Hargreaves, J. K.: The Solar-Terrestrial environment, Cambridge University Press., New York, pp. 208, 1992.

Hofmann-Wellenhof, B., Lichtenegger, H., and Wasle, E.: Global Navigation Satellite Systems, GPS, GLONASS, Galileo and more, Springer Wien New York, pp. 105, 2007.

Jakowski, N., Hoque, M. M., and Mayer, C.: A new global TEC model for estimating trans-ionospheric radio wave propagation errors, J. Geod., 85, pp. 965 - 974, 2011a.

Jakowski, N., Schlüter, S., and Sardon, E.: Total electron content models and their use in ionosphere monitoring, Radio Sci., 46, RS0D18, doi:10.1029/2010RS004620, 2011b.

Leva, J. L., de Haag, M. U., Dyke, K. V.: Performance of standalone GPS. In Kaplan, E. D. and Hegarty, C. J., editors, *Understanding GPS: Principles and Applications*, p. 66 – 112, Artech House INC., 2006.

Mukhtarov, P., Pancheva, D., Andonov, B., and Pashova, L.: Global TEC maps based on GNSS data: 1. Empirical background TEC model, J. Geophys. Res: Space Phys., 118, pp. 4594 - 4608, 2013.

Mungufeni, P., Jurua, E., Habarulema, J. B., and Anguma, S. K.: Modeling the probability of ionospheric irregularity occurrence over African low latitude region, J. Atmos. Sol.-Terr. Phys., 128, pp. 46 - 57, 2015.

Mungufeni, P., Habarulema, J. B., and Jurua, E. a.: Trends of ionospheric irregularities over African low latitude region during quiet geomagnetic conditions, J. Atmos. Sol.-Terr. Phys., 14, pp. 261–267, 2016a.

Mungufeni, P., Habarulema, J. B., Migoya-Orué, Y., and Jurua, E.: Statistical analysis of the correlation between the equatorial electrojet and the occurrence of the equatorial ionisation anomaly over the East African sector, Ann. Geophys., 36, pp. 841 – 853, 2018.

Mungufeni, P., Rabiu, A. B., Okoh, D., and Jurua, E.: Characterization of Total Electron Content over African region using Radio Occultation observations of COSMIC satellites, Adv. Space Res., doi:10.1016/j.asr.2019.08.009, 2019.

Najman, P. and Kos, T.: Performance Analysis of Empirical Ionosphere Models by Comparison with CODE Vertical TEC Maps, Chapter 13, in: Mitigation of Ionospheric Threats to GNSS: an Appraisal of the Scientific and Technological Outputs of the TRANSMIT Project, InTech Open Science publications, pp. 162 - 178, doi:10.5772/58774, 2014.

Nava, B., Coïsson, P., and Radicella, S. M.: A new version of the NeQuick ionosphere electron density model, J. Atmos. Sol. Terr. Phys., 70 (15), pp.1856 – 1862, 2008.

Okoh, D., Owolabi, O., Ekechukwu, C., Folarin, O., Arhiwo, G., Agbo, J., Bolaji, S., and Babatunde, R.: A regional GNSS-VTEC model over Nigeria using neural networks: A novel approach, Geodesy and Geodynamics, 7 (1), pp. 19 - 31, 2016.

Opperman, B.: Reconstructing ionospheric TEC over South Africa using signals from a regional GPS network, Rhodes Univ., Ph. D. Thesis, pp. 30, Grahamstown, South Africa, 2008.

Rama Rao, P. V. S., Jayachandran, P. T., Sri Ram, P., Ramana Rao, B. V., Prasad, D. S. V. V. D., and Bose, K. K.: Characteristics of VHF radiowave scintillations over a solar cycle (1983 - 1993) at a low-latitude station: Waltair (17.7^{o}N, 83.3^{o}E), Ann. Geophys, 15, pp. 729 – 733, 1997.

Rishbeth, H. and Garriot, O. K.: Introduction to Ionospheric Physics, pp 47, Academic Press, New York, 1969.

Schunk, W. R. and Nagy, F. A.: Ionospheres: Physics, Plasma Physics, and Chemistry, pp. 335 396, Cambridge University press, New York, 2nd ed., 2009.

Sun, Y., Liu, J., Tsai, H., and Krankwski, A.: Global ionospheric map constructed by using TEC from ground-based GNSS receiver and FORMSAT-3/COSMIC GPS occultation experiment, GPS solutions, doi:10.1007/s10291-017-0635-4, 2017.

https://doi.org/10.5194/angeo-2019-160
Preprint. Discussion started: 18 December 2019

Annales Geophysicae
Discussions

Tebabal, A., Radicella, S. M., Damtie, B., Migoya-Orue', Y., Nigussie, M., and Nava, B.: Feed forward neural network based ionosphericmodel for the East African region, J. Atmos. Sol. Terr. Phys., 191, pp. 1 – 10, doi:10.1016/j.jastp.2019.05.016, 2019.

Thébault, E., Finlay, C. C., Beggan, C. D., Alken, P., Aubert, J., Barrois, O., Bertrand, F., Bondar, T., and Bones, A.: International Geomagnetic Reference Field: the 12th generation, Earth, Planets and Space, pp. 67-79, doi:10.1186/s40623-015-0228-9, 2015.

Zhang, M.-L., Wan, W., Liu, L., and Ning, B.: Variability study of the crest-to-trough TEC ratio of the equatorial ionization anomaly around120^{o}E longitude, Adv. Space Res., 43, 1762 – 1769, 2009.